Electrodeposited tungsten-rich Ni-W, Co-W and Fe-W cathodes for efficient hydrogen evolution in alkaline medium

E. Vernickaite [a], N. Tsyntsaru [a, *], K. Sobczak [b], H. Cesiulis [a, **]

[a] Department of Physical Chemistry, Vilnius University, Naugarduko str. 24, LT, 03225, Vilnius, Lithuania
[b] Faculty of Chemistry, Biological and Chemical Research Centre, University of Warsaw, Ż wirki i Wigury 101 Str., PL-02-089, Warsaw, Poland

A B S T R A C T

The search of active, stable and cost-effective non-noble electrocatalysts for hydrogen evolution reaction (HER) is essential for sustainable energy systems. In this study, the electrodeposited Ni-W, Co-W and Fe-W coatings having 5–30 at.% of W were examined as an alternative electrocatalysts for hydrogen evo-lution. The electrocatalytic efficiency of the electrodes was investigated on the basis of electrochemical data obtained from steady-state polarization technique in 30 wt% NaOH solution. It was found that with increasing of tungsten content in the deposits up to ~30 at.% a crystal-to-ultra-nanocrystalline transition takes place and the crystal grain size decreases up to 2–4 nm. The high content of W leads to course-grained coatings. These morphological and structural changes showed remarkable impact on the cata-lytic activity. The maximum catalytic performance was obtained for ultra-nanocrystalline W coatings. Among them the Ni-29at.%W demonstrated the highest apparent exchange current density (ECD) at the room temperature, i.e. 0.55 mA cm^{-2}, thus indicating more favorable hydrogen reduction. A significant improvement of catalytic activity of all tested cathodes with increasing the temperature of NaOH solu-tion was noticed. Among investigated Co-33at.%W, Fe-30at.%W and Ni-29at.%W cathodes, the last one showed the best performance towards HER (ECD = 14.5 mA cm^{-2} at 65 °C).

Keywords:
electrodeposition
Tungsten alloys
Iron group metal alloys
Electrocatalysis
Hydrogen evolution reaction

1. Introduction

Hydrogen is a clean, environmentally friendly and renewable energy carrier [1]. Therefore hydrogen generation for energy sys-tems is poised to be the best alternative to depleting fossil fuel reserves in the future [2]. From this point of view electrocatalytic water splitting attracts extensive attention compared to other hydrogen production approaches (e.g. steam reforming, coal gasi-fication) due to its technological simplicity and ecological cleanliness [3], smaller costs [4] and reasonable efficiencies [5]. Consequently, the hydrogen evolution reaction (HER) in both acidic and alkaline media is one of the most explored fields of electro-chemistry. However, application of acidic electrolysis for hydrogen production remains limited by the high cost of proton exchange membranes that are used in an electrolyzer system and low sta-bility caused by corrosion issues [6]. On the other hand, compared with acidic media, HER in alkaline solution generally requires higher overpotentials and is associated with lower efficiency and larger energy consumption. Thus, the effective state-of-the-art catalysts that work well in acidic media can considerable lose the catalytic performance in an alkaline media [7].

Therefore, the water electrolysis industry is mainly focused on improving the efficiency of HER in basic environment by the proper selection of electrode materials that allow enhancing the hydrogen reaction kinetics. The mainstream characteristics that the electrodes should possess: exceptional electrocatalytic activity; good electrical conductivity; low hydrogen overpotential at rather high current densities (1-2 A cm^{-2}); longterm stability during electrolysis process and high corrosion resistance. In this context platinum and other precious metals are unconquerable catalysts, since they are char-acterized by superior surface stability and require very small overpotentials, e.g. e 12 mV to reach the current density of 10 mA cm^{-2} in 1 M KOH and −47 mV in 0.1 M KOH [8]. Unfortunately the deficiency and high price limit their large-scale appli-cation in water electrolysis. This opens the window for alternative, durable, cost-effective materials that would be suitable for replacement of noble metals. Among various alternatives, W(Mo)-based alloys with iron group metals, namely Ni, Co and Fe,

have attracted considerable research attention during the last decades because of their high electrocatalytic activity [9–11], superior mechanical [12,13], tribological [14–16], anti-corrosion properties [15] and thermal resistance [18,19]. W(Mo) alloy electrodes with iron group metals have been prepared by various methods, such as magnetron sputtering [10,20,21], hydrothermal treatment [22], arc melting [23], mechanical alloying [24–27] and electrodeposition [28–30]. Among them, electrodeposition is considered as rather simple and inexpensive technique which does not require a so-phisticated equipment or large energy expenditure. Furthermore, W(Mo)-based alloys prepared by electrodeposition showed the highest electrocatalytic activity and stability in long-term opera-tions [31].

It was reported that Co-W thin films show better performance for the HER than Ni-W deposits [32]. Meantime to the best of our knowledge, no works are available on the electrocatalytic performance of Fe-W alloy as a cathode for alkaline water electrolysis. This could be related to its stability issues under working conditions in terms of corrosion [33]. The ability of an electrode to catalyze the HER is usually measured by the exchange current density (ECD), which is the rate of hydrogen evolution per surface area at the electrode potential, where the reaction is at equilibrium. According to different authors the ECD for Ni-W and Co-W electrodes for the HER in alkaline solution varies in the range of 10^{-5} - 10^{-2} A c m $^{-2}$ [11] and fundamentally depends on corresponding alloy's chemical composition, morphology, structure and physico-chemical properties. It was shown that the ECD rises with increasing W content in Ni-W [20] and Co-W [23] alloys and becomes maximal at 10 at.%. A general explanation of this tendency was based on the local density-functional theory of the transition metal alloys, indicating that the increase in electrochemical activity is attributed to the modification of the density of states of the host metal [23]. The main contribution to the density of states comes from d-electrons. The optimal catalytic activity for the HER on the Ni(Co)-W alloy 10 at.% W coincides with an increase in the density of states at Fermi level of the 3d Ni band. The increased electron density around Ni-sites influences proton discharge at the Ni(Co)–W surface and Ni sites can serve as a hydrogen source for the neighboring W sites in which the ion/atom recombination and molecular hydrogen desorption are promoted more efficiently [20,23]. Similarly in Ref. [34] the best HER activity in 30 wt% NaOH solution was observed for Ni-W alloy having about 14 at.% W (ECD = 0.3 mA cm^{-2}), while the W-richest Ni-W alloy (31.7 at.%) was described as the weakest HER electrocatalyst under the same conditions (ECD = 0.02 · 10^{-2} mA cm^{-2}). These findings agree well with the conclusions in Ref. [10], suggesting that in order to obtain more active W-based electrodes with iron group metals it is necessary to prepare them with less than 19 at.% of W. Although, it is possible to find some controversial information defining the optimal composition of Ni-W or Co-W alloys for the alkaline HER. For instance, a significant improvement in the electrocatalytic efficiency was observed for ultra-nanocrystalline Ni-W electrodes containing >32 at.% of W most likely due to the absorption of a larger amount of hydrogen into their specific structures [35,36]. The positive effect on the catalytic activity for HER of amorphous Ni-W alloys' nature was also confirmed by Ref. [37]. Notable, in the case of Co-W alloys, the ECD for hydrogen evolution as a function of the W content denoted a minimum corresponding to a transition from polycrystalline to nanocrystalline structure, namely at around 25 at.% of W [38]. However, for similar tungsten content (~24–26 at.%) disagreeing results were obtained [39]. Namely, acknowledging the better catalytic performance towards HER in 20 wt% KOH of those coatings. Thus, despite the large amount of research data collected in this field, no univocal dependence of electrocatalytic activity on the chemical composition of the W-based alloy coatings can be determined. The discrepancies in ECDs on alloys with similar chemical composition reported from author to author can be found. This confirms the sensitivity of alloys' characteristics to the provided conditions of electrolysis that influence not only chemical but also phase composition, which in turn, influence the catalytic properties as a whole. Hence, for the first time a comprehensive analysis and comparison of the performance of Ni-W, Co-W and Fe-W alloys (W: from 5 to 30 at.%) which have been prepared from the same initial citrate-based electrolyte by applying the minor changes in elec-trodeposition conditions (in order to obtain similar W content) for the HER in 30 wt% NaOH solution in the temperature range from 25 to 65 °C is presented. The kinetics towards the HER of the as-deposited electrodes was studied by using steady-state polariza-tion measurements.

2. Experimental

2.1. Electrodeposition

Co-W, Ni-W, Fe-W alloy coatings were electrodeposited under galvanostatic mode by using a standard three electrodes configuration. Ag/AgCl/KCl (sat) electrode has been used as a reference electrode (RE) and all potentials presented in this study are referred to this electrode. As a counter electrode (CE) was a platinized titanium mesh (~20 cm^2). Notable, W-based alloys were deposited from non-volatile citrate-borate electrolytes, proposed in our pre-vious works [40,41]. All solutions were prepared from chemicals of analytical grade purity dissolved in distilled water. The pH was adjusted by adding concentrated solutions of NaOH or H_2SO_4. The composition and pH of the applied plating baths used for alloys' electrodeposition are presented in Table 1. The deposits in all cases were obtained at the current density of 10 mA cm^{-2} and temperature of 60 °C. Electrodeposition in all cases was carried out on stainless steel substrate foils (2 cm^2), and on stainless steel rods (1 cm^2), depending on the requirements for coatings' characterization. The stainless steel (with composition in wt.%: Fe-70, Cr-19, Ni-8, Mn-2, Si, Al, P-1) was chosen as a substrate in order to avoid the corrosion. The stainless steel substrate was chemically degreased and cleaned in an ultrasonic bath with acetone, ethanol and finally rinsed with distilled water. In order to improve the adhesion of the alloys to the substrates, a thin nickel seed layer (~30 nm) was electrodeposited from an electrolyte containing 1 M NiCl and 2.2 M HCl, at a cathodic current density of 10 mA cm^{-2} for 1 min. The electrodeposition time for W-based alloys and iron group metals was controlled in a way until the desired coating thickness of around 10 μm was achieved. The given thickness allows to avoid any interference from the stainless steel substrate.

2.2. Structural and morphological characterization

Surface morphology of electrodeposits and chemical composition were examined by scanning electron microscope (SEM, Hitachi SU-70) combined with an INCA energy dispersive X-ray spectroscopy detector (EDS, Oxford Instruments) operated at 20 kV (1 μm penetration depth). After determining the composition of the as-deposited alloys by EDS, the current efficiency (CE) was calcu-lated according to the Faradays' law using following formula:

$$CE\ (\%) = \frac{F \cdot m}{I \cdot t}\left[\frac{x_i \cdot n_i}{M_i} + \frac{x_W \cdot n_W}{M_W}\right] \cdot 100\%, \quad (1)$$

where F - Faradays constant (96485C); m – measured mass (g); I - current flowing through the plating solution (A); t -

Table 1
Composition of the plating baths used for electrodeposition of Ni-W, Co-W, Fe-W alloys; and Co, Ni and Fe coatings.

Coating	W, at.%	Concentration, mol l^{-1}					
		$(Co/Fe/Ni)SO_4$	$C_6H_8O_7$	$Na_3C_6H_5O_7$	H_3BO_3	Na_2WO_4	pH
Co/Ni/Fe	**-**	0.2	0.04	0.25	0.65	–	**6.7**
Co-W	5	0.2	0.04	0.25	0.65	0.2	**5.0**
	20						**6.7**
	30						**8.0**
Ni-W/Fe-W	5	0.04	0.04	0.2	0.16	0.24	**5.0**
	20	0.02					
	30						**6.7**

electrodeposition duration (s); x_i, n_i, M_i – content (wt.%), electron number, molecular weight (g mol^{-1}) of *i-th* component of the alloy (Ni, Co or Fe); x_W, n_W, M_W - content, wt.%, electron number, molecular weight of tungsten (W).

The thickness of the electrodeposits in all cases was around 10–15 μm and was calculated from gravimetric and elemental analysis data using the following equation:

$$d = \frac{m}{A}\left[\frac{x_i \cdot m}{\rho_i} + \frac{x_W \cdot m}{\rho_W}\right], \quad (2)$$

where d – thickness (cm); A – surface area of the cathode (cm^2); ρ_i – density of *i-th* component of the alloy (Ni, Co or Fe) (g cm^{-3}); ρ_i – density of W (g cm^{-3}).

The structural changes of the thin films were analyzed by X-ray diffraction method (XRD: Rigaku MiniFlex II). XRD patterns were produced with Cu Kα radiation (λ = 1.5406 Å) in a 2Θ scanning mode from 20° to 100° with the step of 0.01°. Analysis of the spectra was carried out using PDXL software. The crystallite size of all obtained coatings was calculated based on the broadening of XRD peaks by using Sherrer's equation [42]. The roughness of the deposits was estimated by interpreting the atomic force microscopy (AFM, BioscopeII/Catalyst) results, as their average roughness (R_a). The R_a of the stainless steel substrate was 12 nm before electrodeposition of metals (Co, Ni, Fe) and alloys (Co-W, Ni-W, Fe-W).

Transmission electron microscopy (TEM) results were obtained using a Talos F200X (200 kV, field emission) HRTEM microscope equipped with four detector super-EDS systems (FEI).

2.3. Electrocatalytic evaluation

The electrocatalytic activity of the deposited electrodes towards the HER was evaluated by the following kinetic parameters: the apparent ECD (j_0), the Tafel slope (b_c), the overpotential at the current density of 300 mA cm^{-2} (η_{300}) and the apparent activation energy (E_a). The voltammetric measurements for determining the kinetic parameters of the deposited samples were performed in 30% NaOH solution at 25–65 °C in a thermostated cell. A platinum foil has been used as an auxiliary electrode, and Ag/AgCl/KCl (sat) electrode was used as the reference electrode. The geometrical area of all investigated working electrodes was 1 cm^2 and the experimental results are referred to this geometric surface area. Potentiodynamic polarization hydrogen evolution curves were recorded at the sweep rate of 2 mV s^{-1}. Before starting the measurement, each sample was left in the solution to attain a steady state, which was indicated as open circuit potential (OCP). The cathode potential was scanned from OCP up to −1 V. Voltammetric curves were recorded using potentiostat/galvanostat AUTOLAB equipped with GPES software (version 4.9).

Extrapolation of the polarization curves obtained at different temperatures, in the coordinates $\lg j - \eta$ to the value $\eta = 0$ made it possible to determine the ECD. The overvoltage, η, was calculated from the following equation:

$$\eta = E - E_r, \quad (3)$$

$$E_r = -\left(\frac{2.3RT}{F}\right)\mathrm{pH} \quad (4)$$

where η is an overpotential of the HER (V), E is an experimental potential value at which the reaction takes place (V); E_r is the reversible potential value calculated from the Nernst equation (V), R is the universal gas constant (8.3144 J K^{-1} mol^{-1}); T is the temperature (K); F is the Faraday constant (96 485 J mol^{-1}).

For the calculation of overpotentials at temperatures other than 25 °C, the tabulated data [43] of the temperature dependence of the potential of the saturated Ag/AgCl/KCl (sat) electrode vs. the hydrogen electrode, were used.

The oxide film layer formed in the 30 wt% NaOH solution was investigated using the electrochemical impedance spectroscopy (EIS). The thickness of the oxide layer was calculated from the capacitive behavior of the film by using the relation:

$$d = \frac{\varepsilon_0 \varepsilon_r S}{C} \quad (5)$$

where d is the thickness of the oxide layer (m), C is the capacitance of the oxide layer (F), S is the surface area (m^2), ε_0 is the electric constant ($\varepsilon_0 \approx 8.854 \times 10^{-12}$ F m^{-1}); ε_r is the dielectric constant of Co/Ni/Fe and W oxides.

Because the dielectric constants of iron group metals (Co, Ni, Fe) and W significantly differ, the total ε_r was calculated using the following equation:

$$\varepsilon_r = x_{Me}\varepsilon_{MeO} + x_W\varepsilon_{WO_3} \quad (6)$$

where x_{Me} and x_W are atomic fractions of iron group metal (Ni, Co, Fe) and tungsten in the corresponding alloy, respectively. Taking $\varepsilon_r = 11.9$; 12.9 and 14.2 for NiO, CoO and FeO, respectively, and $\varepsilon_r = 300$ for WO_3.

3. Results and discussion

3.1. Characterization of Ni-W, Co-W and Fe-W alloy coatings

Morphology. The electrocatalytic activity of alloys depends on the surface roughness that enhances the specific surface area available for the HER [44]. Consequently, both alloy composition and surface morphology determined by electrolysis conditions have remarkable influence on the catalytic activity. Based on reports [45–47] certifying that the catalytic activity for hydrogen evolution is qualitatively proportional to the refractory metal (W/Mo) content in the alloys with iron group metals (Ni, Co, Fe) the main approach of this work was to increase the W content in Ni-W, Co-W and Fe-W coatings, namely from 5 to 30 at.%, and thereby to

investigate its influence on electrocatalytic performance towards HER. In order to vary the composition of alloys the pH of the corresponding plating bath was changed in the range of 5.0 ÷ 8.0 (Table 1). The influence of pH on the chemistry of electrolytes and composition of W alloys with the iron group metals are comprehensively described in Refs. [40,48]. In order to compare the electrocatalytic properties of the obtained W-alloys, Ni, Co and Fe also were deposited under the same electrolysis conditions. In this case the pH of 6.7 chosen for electrodeposition, because it is an initial value which is settled after mixing the components of corre-sponding solutions. The representative SEM top-view images of the various compositions of Ni-W, Co-W and Fe-W alloys along with Ni, Co and Fe metals for comparison are shown in Table 2.

As it can be seen, the iron group metal coatings have the surface morphology clearly different from their binary alloys with W. In general, with increasing the W content a transition in the surface morphology from the deposits with angular/facetted structure (characteristic to Ni, Co and Fe) to nodular nature coatings (specific to W-rich alloys) was determined. Notable, the alloys are characterized by more homogenous and denser morphology. The surface roughness measurements (Table 3) further reveals that the addition of W can smooth the Ni-W and Fe-W alloy surfaces. In these cases the average surface roughness (R_a) decreases from ~600 to 700 nm (for iron group metals) to ~ 300 nm (at 30 at.% W). These observations are in a good agreement with the characteristics expected for ultra-nanocrystalline alloys with increased W content in the alloy's composition [49–51]. Unlike, the R_a of electrodeposited Co-W coatings shows the tendency to increase with the higher W percentage in the alloy's composition and attain its maximum for Co-33at.%W ($R_a = 487$ nm). The "cauliflower" type structures that appear as aggregates of the smaller grains are clearly observed in the SEM picture of this surface.

Table 3
The average roughness, current efficiency and grain size of the as-deposited coatings.

Sample	Roughness, nm	Current efficiency, %	Grain size, nm
Ni	686	47.6	22.7
Ni-5 at.% **W**	639	44.2	14.9
Ni-20 at.% **W**	397	31.1	10.0
Ni-30 at.% **W**	270	21.8	4.3
Co	322	91.3	33.7
Co-4 at.% **W**	171	89.6	27
Co-20 at.% **W**	416	83.0	23.7
Co-33 at.% **W**	487	35.5	1.5
Fe	556	66.5	41.8
Fe-5 at.% **W**	410	50.2	21.4
Fe-20 at.% **W**	256	46.9	1.5
Fe-31 at.% **W**	310	37.4	1.5

It is well known that the electrodeposition of W-based alloys from aqueous electrolytes occurs with the significant hydrogen release, resulting in the distortion of coating's structure due to the hydrogen saturation, which provokes the cracking of the coatings [52]. The presence of the microcracks on the surface results in a decrease of fatigue life and localized corrosion problem that is one of the main limitations of using W alloy coatings for the target purposes [15,28]. Though there is some data declaring that the

Table 2
SEM micrographs of Ni, Co, Fe and Ni-W, Co-W, Fe-W electrodeposits made at higher (x6000) and lower (x500, inserts) magnifications.

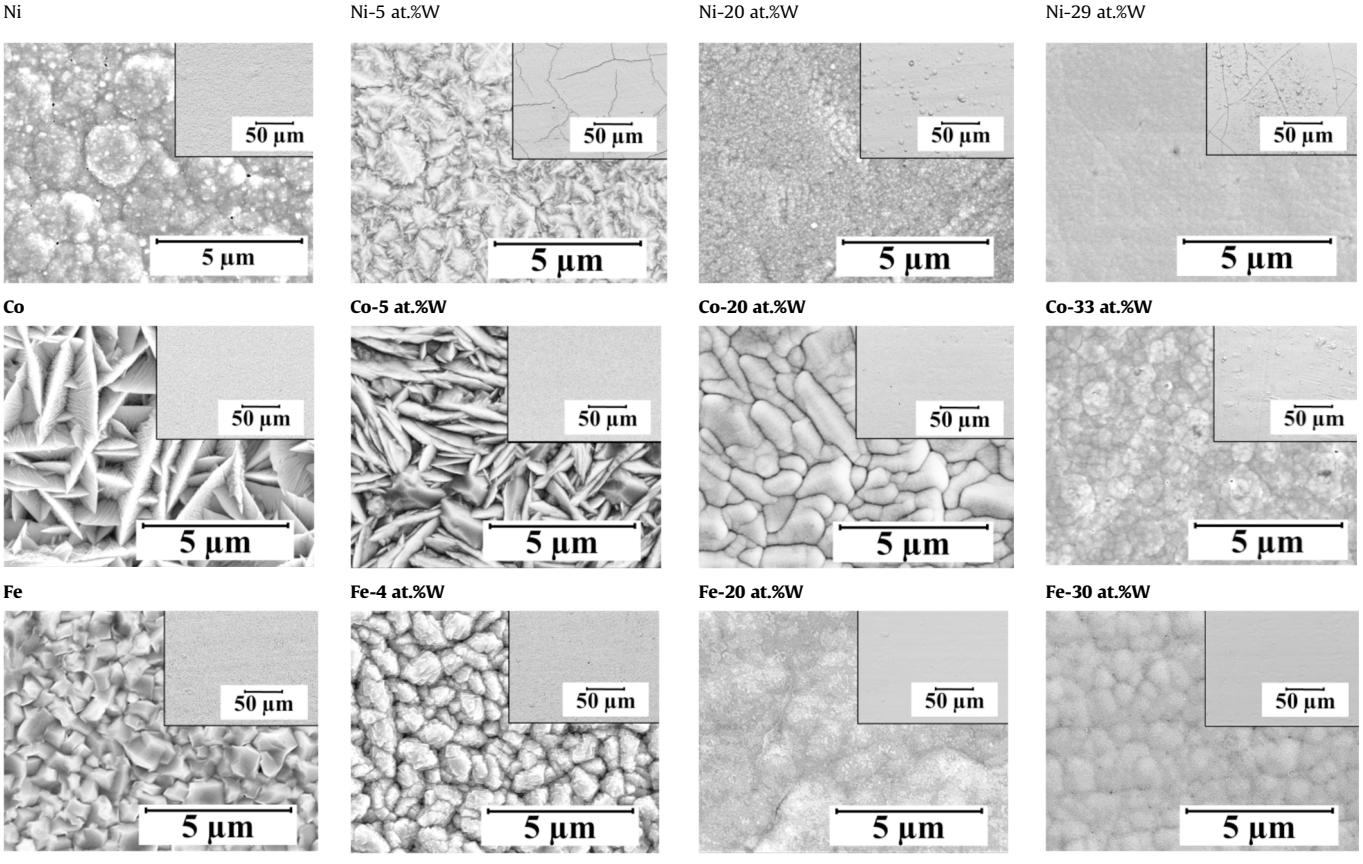

formation of the microcracks leads to the higher electrocatalytic activity of electrode for HER. The reason behind that cracks, being filled with electrolyte, render a greater part of the internal surface of the electrode accessible to electrochemical gas evolution [53,54]. From the SEM images made at lower magnification the presence of the cracks on Ni-W surfaces at 5 and 29 at.% W can be noticed, whilst the electrodeposited Co-W and Fe-W coatings having similar composition are uniform and no cracks can be observed (Table 2). This could be attributed to the lower cathodic current efficiency of Ni-W alloys (Table 3), and consequently, more intensive hydrogen evolution during the deposition due to the higher initial Ni catalytic activity towards HER in comparison with the Co and Fe. The Ni-5 at.% W coating has the cracking pattern characterized by the highest density. Since the formation of spherical nodular structure becomes more favorable for Ni-29at.% W, the crack density de-creases. Similar observations have been made in Ref. [28].

Structure. The catalytic activity of electrodes is also strongly influenced by their crystal structure, especially, nanocrystalline or amorphous states have been reported as the most attractive towards HER [35]. Furthermore, amorphous alloys are known to exhibit higher hardness, better tribological properties [55] and also a better corrosion behavior compared to those of crystalline ones [56]. The X-ray diffraction (XRD) spectra of the deposits are given in Fig. 1. It was established that the crystallinity of W alloys with iron group metals is associated to W content, i.e. Ni-W and Co-W coatings with a low tungsten percentage ($\leq$22 at.%) have the crystalline structure and coatings with the higher tungsten content are ultra-nanocrystalline. Notable, the crystalline to ultra-nanocrystalline transition for Fe-W alloy is occurs at lower W content, namely 15−17 at.%, that value is slightly lower than it was reported by other authors [24,57]. The alloys having low-W content did not show any evidence of additional diffraction lines relating to elemental tungsten or W- compounds, only those for hcp Co, fcc Ni or bcc Fe lattice. Furthermore, a shift of Co, Ni and Fe peaks towards smaller diffraction angles is observed. This suggests that during tungsten co-deposition with iron group metals bigger W atoms are incorporated into crystalline lattice of Ni, Co or Fe and corresponding solid solutions are formed. These observations agree with the previous works in which W-based alloys were prepared from gluconate or saccharin containing bath [30,58,59]. Meanwhile at the high tungsten content (~30 at.% for Ni-W and Co-W; $\geq$ 20 at.% for Fe-W) the single broad peaks revealing the ultra-nanocrystalline (the crystallite size is less than 4 nm) structure can be observed. In the literature it is widely described that such peak broadening is attributed to the reduction of the crystallite size of an alloy with an increase in the amount of tungsten [40,51]. Indeed, the crystallite sizes decreases from 27 nm to ~1.5 nm for Co-W alloy; from 15 to ~4 nm for Ni-W alloy; from 41 nm to ~1.5 nm for Fe-W alloy with increasing the W percentage from 0% (iron group metals) to 30 at.% (Table 3). However, in the case of the broad peak in XRD pattern it is difficult to strictly determine to which phase it is attributed. Nevertheless, based on the equilibrium phase diagrams [60−62] and previous investigations, it can be assumed that the W solid solutions in Ni, Co or Fe together with their corresponding thermodynamically stable intermetallic phases of Co_3W [40,63], Fe_2W [57], Ni_4W [17, 64]. It was shown that different intermetallic phases have an impact on their activity for the HER [65,66].

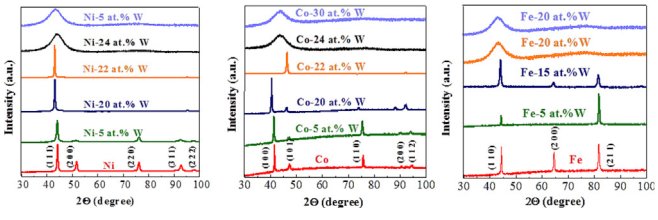

Fig. 1. XRD patterns of as-deposited Ni, Co, Fe and Ni-W, Co-W, Fe-W coatings. Composition of alloys is given in at.%.

The values of crystallite sizes is confirmed by diffraction patterns obtained by TEM (see Fig. 2). It shows that alloys consist of few nanometers sized crystallites, and the crystallinity of Co-W alloy is more evident in comparison with Ni-W alloy.

The metal distribution was also examined. Here we present the characteristic results obtained for NiW alloy. As it seeming from comparison of the TEM images of Ni-W alloy spot presenting mapping of elements (see Fig. 3), both Ni and W are present onto entire sample (see Fig. 3 c and d). However, as it is shown in Fig. 3 b, there are some regularly located (several nanometers in diameter) spots with significantly higher amount of W are present. It was also proved that the spots with higher concentration of W are crystal-line (see inset in Fig. 3a). The TEM results suggest that material obtained in electrodeposition process consists of two phases: tungsten solution in nickel (amorphous phase with lower tungsten content) and intermetallic, crystalline phase of intermetallic com-pounds containing higher percentage of tungsten, e.g. NiW. Detailed identification of the stoichiometry of the crystalline phase require more advanced TEM and XRD measurements and will be a subject of further examination.

3.2. Electrocatalytic hydrogen evolution on Ni-W, Co-W and Fe-W coatings

The steady-state equilibrium method is one of the simplest techniques for investigating the electrocatalytic activity in the alkaline water electrolysis [67]. Hence, in order to investigate the catalytic activity of the prepared Ni-W, Co-W and Fe-W electrocatalysts having different W content, linear sweep voltammetry measurements were performed in 30 wt% NaOH solution at 25 ± 2 °C. The polarization curves of the investigated samples are presented in Fig. 4(a−c). The corresponding electrochemical parameters (Tafel slope (b_c), apparent exchange current density (j_0), and overpotential at j = - 200 mA cm^{-2} (η_{200})) obtained from the linear part of semi-logarithmic polarization plots (Fig. 4(d and e)) are summarized in Table 4. The comparative studies were performed on the electrodeposited Ni, Co and Fe coatings and metallurgical Pt under the same experimental conditions. It was found that Tafel slopes vary in the range from - 185 to - 142 mV dec^{-1} for Ni-W, from - 189 to - 146 mV dec^{-1} for Co-W and from - 233 to - 176 mV dec^{-1} for Fe-W alloy coatings with increasing the W percentage from 0 to ~30 at.%. These values are in a good agreement with previous works based on W(Mo) and iron group metal

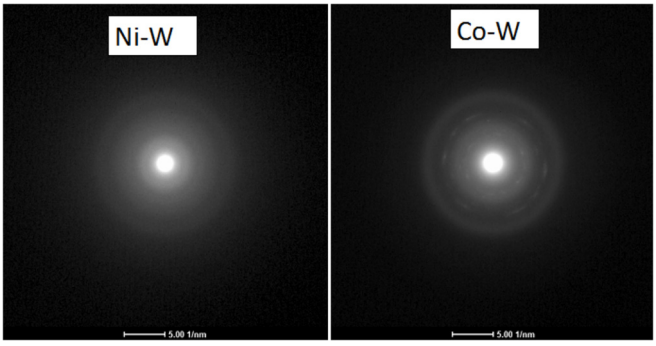

Fig. 2. Diffraction patterns obtained by high resolution TEM of Ni−29at.% W and Co−33at.%W alloys.

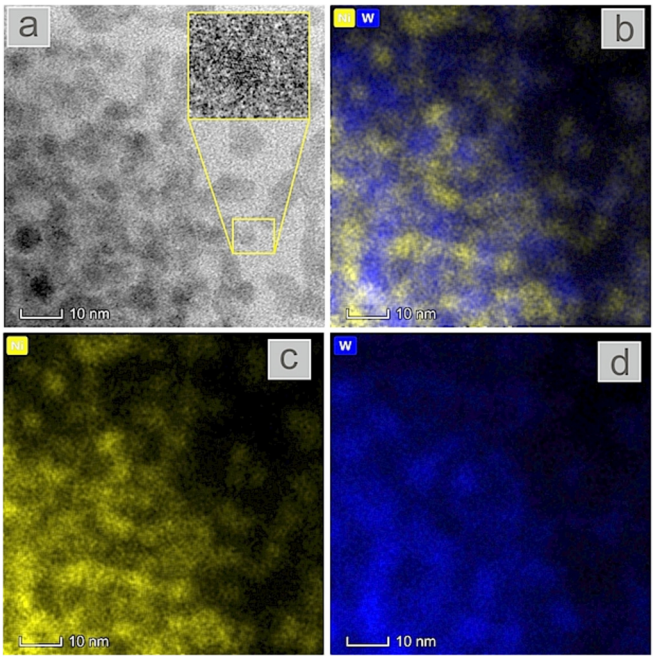

Fig. 3. High resolution TEM images of the Ni-W sample; (a) bright field TEM image of examined spot; (b) EDX map of Ni and W distribution; (c) EDX map of Ni distribution; (d) EDX map of W distribution.

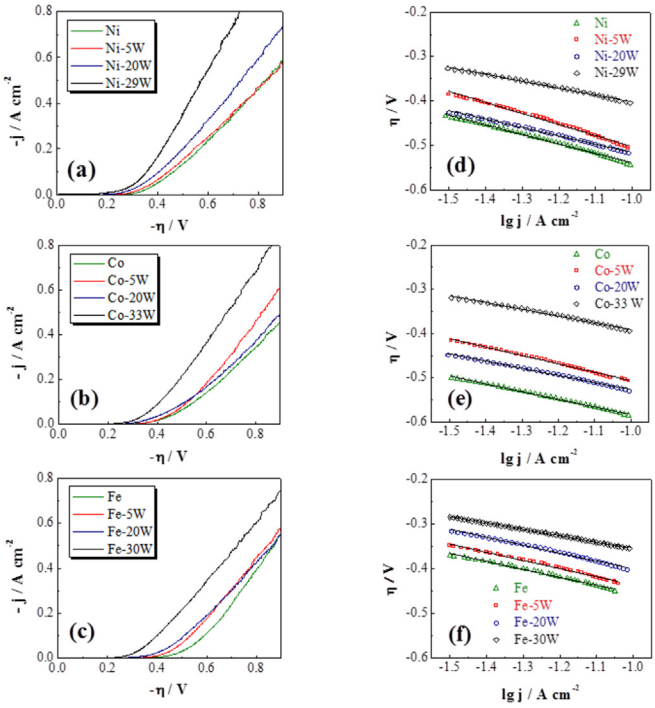

Fig. 4. Cathodic polarization curves of hydrogen evolution in 30 wt% NaOH at 25 ± 2 °C for electrodeposited coatings with different chemical compositions (a–c) and the plots in semi-logarithmic coordinates (d–f). The scan rate is 2 mV s^{-1}. The composition of alloys are given in at.%.

catalysts for the HER [23,31,68,69]. It is widely accepted that the HER kinetics in alkaline medium involves the electron-coupled water dissociation (the Volmer step for the formation of adsorbed hydrogen) and the combination of adsorbed hydrogen into molecular hydrogen via either the interaction of the H atom and water

Table 4
Electrochemical parameters at 25 ± 2 °C for as-deposited coatings and metallurgical Pt.

Electrode	b_c/mV dec^{-1}	j_0/mA cm^{-2}	η_{200}/mV
Ni	185	$1.5 \cdot 10^{-2}$	- 586
Ni-5 at.%.**W**	175	$2.4 \cdot 10^{-2}$	- 584
Ni-20 at.%.**W**	160	$7.3 \cdot 10^{-2}$	- 503
Ni-29 at.%.**W**	142	$5.5 \cdot 10^{-1}$	- 419
Co	189	$3.5 \cdot 10^{-3}$	- 664
Co-5 at.%.**W**	184	$1.6 \cdot 10^{-2}$	- 621
Co-20 at.%.**W**	176	$3.8 \cdot 10^{-2}$	- 611
Co-33 at.%.**W**	146	$2.3 \cdot 10^{-1}$	- 490
Fe	233	$1.0 \cdot 10^{-3}$	- 673
Fe-5 at.%.**W**	204	$1.9 \cdot 10^{-3}$	- 637
Fe-20 at.%.**W**	182	$9.1 \cdot 10^{-3}$	- 517
Fe-30 at.%.**W**	176	$1.6 \cdot 10^{-2}$	- 488
Pt	122	$2.6 \cdot 10^{1}$	- 363

molecule (Heyrovsky step), or the combination of two H atoms (Tafel step) [70]. Each step can determine the overall rate of the reaction. According to this general model, the Tafel slope of 118 mV dec^{-1} at 20 °C indicates that the process is controlled by the Volmer reaction step. While if the Tafel slope is ~40 or ~30 mV dec^{-1}, the rate-determining step would be Heyrovsky or Tafel reactions, respectively [47]. Table 4 shows the Tafel slopes are close to 118 mV dec^{-1}, and thus indicating that the Volmer reaction step is the controlling step of the HER in the alkaline solution in this study. The Tafel slopes greater than the theoretically predicted is related to the presence of the barrier-type oxide film on the electrode surfaces that causes additional potential drop [31,47]. The smaller Tafel slopes indicate the minor change in electrode overpotential for the larger increase in HER current. According to this can be assumed that the W-rich (~30 at.%) electrodes are characterized by faster hydrogen gas production.

At the same time, the apparent ECD values on the active electrocatalyst are desired to be as large as possible, because the higher ECD reflects the faster kinetics toward the redox reaction, i.e. lower overvoltage must be applied to create a significant current flow [71]. It was found that the apparent ECDs on binary W alloys are considerably higher than in the case of Ni, Co and Fe electrodeposits (see Table 4). Especially higher values of the hydrogen evolution rate were observed with increasing W content in the coatings. As it was shown in previous section, W-rich (~30 at.%) alloys are char-acterized by a refined grained (ultra-nanocrystalline) structure that probably offer the greater activity due to the better dispersion of the catalyst active sites and higher affinity for hydrogen absorption [35,72]. Indeed, both increased surface area and intrinsic reactivity can have significant effect on the enhanced catalytic behavior of a target material. Thus, in order to evaluate the intrinsic activity of the electrode in the HER, it is very important to estimate it's real electrochemically active area. However, in our case the higher roughness of the electrode surface that has been observed by SEM imaging and surface topography measurements for the alloys rich in iron group metals (Ni, Co, Fe) did not show the enhancement of the electrochemically active surface area. Contrary, the most active W-rich electrodes characterized by relatively low surface rough-ness (~300 nm for Ni-30at.%W and Fe-31at.%W), compact and ho-mogenous morphology, without any pronounced pores or cavities demonstrated the highest catalytic activity. This phenomenon is comprehensively described in Ref. [73] where it is concluded that the geometric effects of the alloys can be used only for a 'fine-tuning' of the catalytic behavior. Hence, the main factor influencing outstandingly high electrocatalytic activity of the W(Mo) alloys

with iron group metals towards HER could be explained by the synergistic electronic effects [74]. Generally, it was explained that the metals of the left half of the transition series in the periodic table with empty or less-filled d-orbitals (e.g. W/Mo) are alloyed with metals of the right half of the series with more filled d-bands (e.g. Ni, Co, Fe) and the maximum in bond strength and stability of the intermetallic alloy phases is expected [75,76]. Although the corresponding intermetallic compounds are formed in all W-based alloys at the highest co-deposited W content, the influence of the iron group metal nature on the apparent hydrogen ECDs can be noticed. Ni-29at.%W coatings have shown to be the best overall catalyst. Notable, in Ref. [35] the higher catalytic activity of the ultra-nanocrystalline Ni-W alloy was proposed to occur due to the presence of cracks or/and discontinuities on the surface that lead to the higher affinity for hydrogen absorption. Meanwhile in our case even the crack-free Ni-20at.%W electrodeposit showed the higher apparent ECD compared to Co-20at.%W and Fe-20at.%. This suggests that the surface area of the cathode is not the main factor which controls the catalytic behavior. Thus, the origin of the enhanced electrocatalytic activity of Ni-29at.%W could be attributed to the structure peculiarities, more specifically the presence of the intermetallic Ni_4W phase which in previous works was characterized by the fast water dissociation kinetics that allows improving of the HER performance [77]. Indeed, the computational and experimental results revealed the fact that the kinetic energy barrier of the initial Volmer step is substantially reduced on the such type intermetallic phase catalysts [77]. What is more, it was demonstrated that Ni_4W phase is more stable under liquid phase reactions [78,79]. Finally, based on the bipolar electrodes method calculations [80] was concluded that Ni-based electrodes produce the higher number of active sites for the HER than those containing Co and Fe. These assumptions correspond well to previous works reporting the higher catalytic activity for refractory metal alloys with Ni than those containing Co in their composition [81,82]. Notable, the apparent ECD values of Fe-W alloys are of magnitude lower than those determined for Ni-W and Co-W deposits with the analogous compositions (Table 5). This can be related to the higher iron-based compounds affinity to the oxygen and formation of the natural oxide film on the surface which leads to the reduced conductivity [83]. Whilst oxygen affinity for Ni and Co is less than for Fe [84]. Thus, the least compact oxide film is expected to form on Ni-W alloys [85]. To sum up, the apparent ECDs of ultra-nanocrystalline W coatings are higher than that of crystalline ones and the most active electrodes follow the sequence: Ni-29 at.%W > Co-33 at.%W > Fe-30 at.% W.

It is known that the ECD characterizes the electrocatalytic activity of the electrode at equilibrium conditions. However, a certain current density is required for the HER to proceed at a measurable rate. Therefore, in order to compare the electrocatalytic activity of electrodes, it has been suggested to compare rather the overvoltage at the fixed current density [86]. In the light of these facts, in this study the overpotentials at - 200 mA cm^{-2} (η_{200}) were investigated in order to compare the apparent activity of the electrodeposited tungsten-based alloys. The results showed that the overpotential reduction at the above mentioned current density for all coatings follows the sequence of chemical composition: iron group metals >5 at.%W > 20 at.%W > ~30 at.%W, thereby confirming the previous conclusions that the ultra-nanocrystalline electrodes are characterized by the highest electrocatalytic activity for the HER in 30 wt% NaOH at 25 ± 2 °C.

Effect of electrolyte temperature. It is known that the temperature of alkaline bath plays an important role on the increase of the catalytic activity of W(Mo)-based cathodes towards the HER [11,87]. Hence, the electrodeposited Ni-29at.%W, Co-33at.%W and Fe-30at.%W alloy electrodes that demonstrate the higher apparent catalytic activity were tested at the temperature range from 25 to 65 °C by applying 10 °C increments. The characteristic polarization curves obtained for the HER in 30 wt% NaOH on the different electrodes at 25, 45 and 65 °C are displayed in Fig. 5 (a, c, e). Kinetic parameters determined from the linear part of the Tafel curves (Fig. 5 (b, d, f)), i.e. apparent exchange current density, Tafel slopes, and η_{200} are presented in Table 5. The higher temperature exhibits the significant effect on the HER, leading to the distinct reduction of Tafel slopes which is opposite the prediction of classical theory. Apparently, the catalytic activity depends not only on the synergistic effect and/or increased surface area, but also on the surface characteristics.

It was determined that an increase in the bath's temperature induces the formation of a thicker oxide layer, i.e. from 0.02 to 0.7 Å for Ni-29at.%W, from 0.1 to 0.46 Å for Co-33at.%W, from 2.6 to 7.1 Å for Fe-30at.%W. As revealed by XPS analysis [17], the electrodeposited iron group metals alloys of high W-content are covered with a surface layer of the tungsten-based oxides. It is known that tungsten oxide, WO_3, has been long accepted as a promising non-precious-metal electrocatalyst for hydrogen

Table 5
Experimental values of the apparent ECD (j_0, mA cm^{-2}) and Tafel slopes (b_c, mV dec^{-1}) for as-deposited alloy electrodes at different temperatures (composition is given in at.%).

Electrode	25 °C		35 °C		45 °C		55 °C		65 °C	
	j_0	b_c	j_0	b_c	j_0	b_c	j_0	b_c	j_0	b_c
Ni-29 W	0.55	142	1.5	134	2.9	118	5.9	97	14.5	78
Co-33 W	0.29	146	0.91	139	1.2	134	2.7	101	6.0	93
Fe-30 W	0.016	176	0.019	160	0.041	149	0.12	143	0.29	139

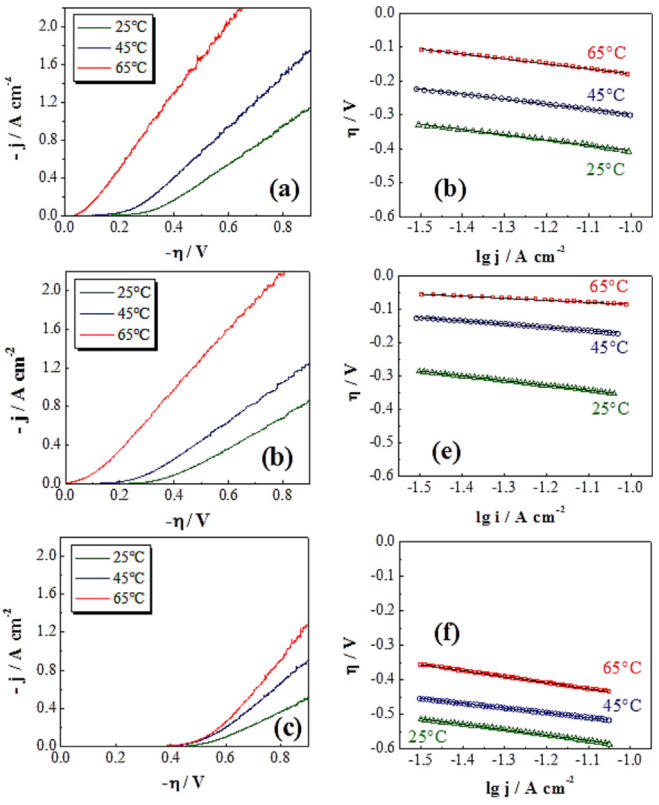

Fig. 5. Influence of the temperature on cathodic polarization curves and plots in semi-logarithmic coordinates for Ni–29at.%W (a–b), Co-33at.%W (c–d), Fe-30at.%W (e–f) electrodeposits. The scan rate is 2 mV s^{-1}.

production [90]. Thus, can be assumed that during the HER at the higher temperature of the solution the thicker oxide layer characterized by catalytic activity results in the lower Tafel slopes. Also the oxide layer can influence the process of hydrogen adsorption. On this basis the real contribution of oxides for catalytic activity is yet another area of enquiry for future investigation. In addition, there is a significant increase in the apparent ECD for all investigated ultra-nanocrystalline electrodes towards HER with increasing temperature. The highest apparent ECD of 14.5 mA cm^{-2} and the lowest Tafel slope of 78 mV dec^{-1} presented in Table 5 were determined for Ni-29at.%W sample at 65 °C, indicating that this catalyst is the most active for the HER among the Co-33at.%W and Fe-30at.%W under similar conditions. This was confirmed by the lower overpotential value at −200 mA cm^{-2} determined for Ni-29at.%W electrode (η_{200} = - 120 mV) than that determined for Co-33at.%W and Fe-30at.%W (η_{200} = - 146 and - 429 mV, respectively). For comparison, the apparent ECD obtained for metallurgical Pt was 9.1 mA cm^{-2} with the Tafel slope value of 119 mV dec^{-1} and η_{200} of 106 mV at 65 °C.

In order to better compare the electrocatalytic activity of the most active ultra-nanocrystalline W alloy electrodes, the apparent activation energy (E_a) for the HER in accordance with the Arrhenius relation (Fig. 6) was also estimated. The calculations revealed the following activation energies: 23.5 kJ mol^{-1} for Ni-29at.%W, 26.0 kJ mol^{-1} for Co-33at.%W and 29.8 kJ mol^{-1} for Fe-30at.%W. It is known that the lower the E_a value is, the lower the energy requirements for hydrogen production are. Hence, the above mentioned results suggest the best catalytic performance of electrodeposited Ni-29at.%W catalyst which is highly comparable to that for Pt under the similar experimental conditions (E_a = 19.2 kJ mol^{-1}).

Notable, the apparent ECDs for W alloys towards HER at 65 °C found in this study in some cases seem to be much higher than that in other works, implying higher catalytic activity of the electrodeposited coatings (Table 6). This could be related to the different experimental conditions, i.e. higher concentration of the alkaline solution, elevated bath temperature, surface condition, etc. Nevertheless, the obtained results are of a significant importance, because the enhanced catalytic performance described above

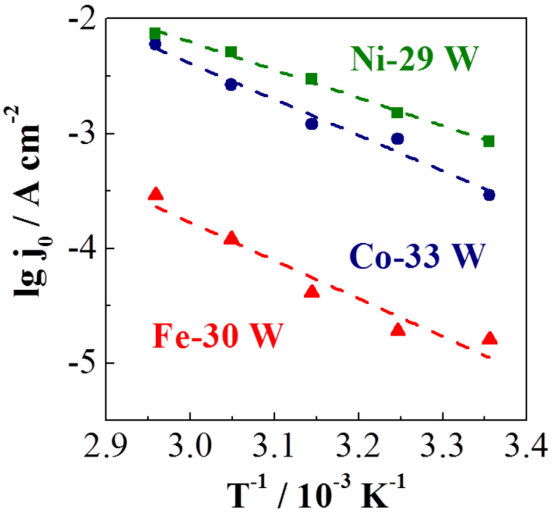

Fig. 6. Arrhenius plots for ultra-nanocrystalline Ni–29at.%W, Co–33at.%W and Fe–30at.%W alloys.

Table 6
Comparison of the ECDs derived from the literature for W-based alloy electrodes.

Sample	W content, at.%	Media	j_0, mA cm^{-2}	Reference
Co-W	18.9	1.0 KOH, 65 °C	$1.1 \cdot 10^{-2}$	[11]
Co-W	10	1.0 M NaOH, 25 °C	$7.65 \cdot 10^{-2}$	[23]
Co-W	27.3	1 M NaOH	$1.13 \cdot 10^{-2}$	[89]
Co-W	22.6	30 wt% KOH, 25 °C	$1.2 \cdot 10^{-3}$	[32]
Ni-W	18.1		$6.5 \cdot 10^{-3}$	
Ni-W	10	1.0 M NaOH, 30 °C	$5.0 \cdot 10^{-2}$	[20]
Ni-W	Not specified	30 wt% KOH, 80 °C	2.83	[75]
Ni-W	40	33 wt% KOH, 25 °C	143.5	[35]
Ni-W	29	30 wt. NaOH, 65 °C	14.5	This work
Co-W	33		6.0	
Fe-W	30		$2.9 \cdot 10^{-1}$	

supplements the previous findings showing the outstanding mechanical [14,40], anti-corrosion [28,88] of W-rich alloys and allows proposing them as suitable materials not only for effective cathodes for HER, but also for the design of the electrodes with multifunctional capability.

4. Conclusions

The electrocatalytic performance of electrodeposited Ni-W, Co-W and Fe-W alloys (0 ÷ 30 at.% W) as the effective cathodes for the HER was investigated using linear voltammetry technique in 30 wt % NaOH at the temperatures ranging from 25 to 65 °C. It was found that alloying of Ni, Co, Fe with W results in the increased electrocatalytic activity towards HER when compared to single iron group metals. Furthermore, it was demonstrated that the higher content of W results in an enhanced HER catalytic activity and electrodes with ~30 at.% of W demonstrated the lowest η_{200} values and the highest apparent ECDs at 25 °C. This could be related to the formation of the stable ultra-nanocrystalline intermetallic compounds and the occurrence of a so-called synergistic effect. At the elevated temperature of NaOH solution a significant improvement of catalytic activity leading to the distinct reduction of the overpotential and the enhancement of the apparent ECD of the ultra-nanocrystalline cathodes was noticed. The apparent ECD values at 65 °C reduced in the following order: Ni-29at.%W>Co-33at.%W>Fe-30at.%W. Moreover, the Ni–29at.%W electrode was characterized by the lower activation energy (23.5 kJ mol^{-1}) than the Co–33at.% W (26.0 kJ mol^{-1}) and Fe–30at.%W (29.8 kJ mol^{-1}) coatings. Such catalytic activity of Ni-29at.%W that is comparable to that of metallurgical Pt probably could be link to the higher number of active sites for the HER and stability of intermetallic Ni_4W phase.

Acknowledgements

This research has received funding from Horizon 2020 research and innovation program under MSCA-RISE-2017-778357-SMARTELECTRODES and from the Research Council of Lithuania, agreement No 09.3.3-LMT-K-712-08-0003. The TEM images were obtained using the equipment purchased within CePT Project No.: POIG.02.02.00- 14-024/08-00. Authors thanks Prof. Mikolaj Donten from Faculty of Chemistry, University of Warsaw (Poland) for valuable discussions.

References

[1] A. Züttel, A. Borgschulte, L. Schlapbach, O. Friedrichs, Hydrogen as a future energy carrier, Phil. Trans. R. Soc. A 368 (2010) 3329.
[2] A.G. Stern, A new sustainable hydrogen clean energy paradigm, Int. J. Hydrogen Energy 43 (2018) 4244.
[3] S.E. Hosseini, M.A. Wahid, Hydrogen production from renewable and sustainable energy resources: promising green energy carrier for clean development, Renew. Sustain. Energy Rev. 57 (2016) 850.
[4] I. Vincent, D. Bessarabov, Low cost hydrogen production by anion exchange

membrane electrolysis: a review, Renew. Sustain. Energy Rev. 81 (2018) 1690.
[5] V.M. Nikolic, G.S. Tasic, A.D. Maksic, D.P. Saponjic, S.M. Miulovic, M.P. Marceta Kaninski, Raising efficiency of hydrogen generation from alkaline water electrolysis – energy saving, Int. J. Hydrogen Energy 35 (2010) 12369.
[6] Y. Naimi, A. Antar, Hydrogen Generation by water electrolysis, in: M. Eyvaz (Ed.), Adv. Hydrog. Gener. Technol., InTech, 2018.
[7] N. Mahmood, Y. Yao, J.W. Zhang, L. Pan, X. Zhang, J.J. Zou, Electrocatalysts for hydrogen evolution in alkaline electrolytes: mechanisms, challenges, and prospective solutions, Adv. Sci. 5 (2018) 1700464.
[8] B. Lu, L. Guo, F. Wu, Y. Peng, J.E. Lu, T.J. Smart, N. Wang, Y.Z. Finfrock, D. Morris, P. Zhang, N. Li, P. Gao, Y. Ping, S. Chen, Ruthenium atomically dispersed in carbon outperforms platinum toward hydrogen evolution in alkaline media, Nat. Commun. 10 (2019) 631.
[9] E. Vernickaite, O. Bersirova, H. Cesiulis, N. Tsyntsaru, Design of highly active electrodes for hydrogen evolution reaction based on Mo-rich alloys electrodeposited from ammonium acetate bath, Coatings 9 (2019) 85.
[10] A. Kawashima, E. Akiyama, H. Habazaki, K. Hashimoto, Characterization of sputter-deposited Ni-Mo and Ni-W alloy electrocatalysts for hydrogen evolution in alkaline solution, Mater. Sci. Eng. A 226–228 (1997) 905.
[11] M.P. Marceta Kaninski, S.M. Miulovic, G.S. Tasic, A.D. Maksic, V.M. Nikolic, A study on the Co–W activated Ni electrodes for the hydrogen production from alkaline water electrolysis – energy saving, Int. J. Hydrogen Energy 36 (2011) 5227.
[12] K.R. Sriraman, S.G. Sundara Raman, S.K. Seshadri, Synthesis and evaluation of hardness and sliding wear resistance of electrodeposited nanocrystalline Ni–Fe–W alloys, Mater. Sci. Technol. 22 (2006) 14.
[13] A. Mulone, A. Nicolenco, J. Fornell, E. Pellicer, N. Tsyntsaru, H. Cesiulis, J. Sort, U. Klement, Enhanced mechanical properties and microstructural modifications in electrodeposited Fe-W alloys through controlled heat treatments, Surf. Coating. Technol. 350 (2018) 20.
[14] F. Su, P. Huang, Microstructure and tribological property of nanocrystalline Co–W alloy coating produced by dual-pulse electrodeposition, Mater. Chem. Phys. 134 (2012) 350.
[15] L. Xu, H. Guan, D. Li, L. Wang, Tribological properties of electroplated crack Ni–W alloy coatings, Proc. Inst. Mech. Eng. Part J J. Eng. Tribol. 229 (2015) 1372.
[16] A. Mulone, A. Nicolenco, N. Imaz, V. Martinez-Nogues, N. Tsyntsaru, H. Cesiulis, U. Klement, Improvement in the wear resistance under dry friction of electrodeposited Fe-W coatings through heat treatments, Coatings 9 (2019) 66.
[17] M. Obradovic, J. Stevanovic, A. Despic, R. Stevanovic, J. Stoch, Characterization and corrosion properties of electrodeposited Ni-W alloys, J. Serb. Chem. Soc. 66 (2001) 899.
[18] N. Tsyntsaru, H. Cesiulis, A. Budreika, X. Ye, R. Juskenas, J.-P. Celis, The effect of electrodeposition conditions and post-annealing on nanostructure of Co–W coatings, Surf. Coating. Technol. 206 (2012) 4262.
[19] N. Sunwang, P. Wangyao, Y. Boonyongmaneerat, The effects of heat treatments on hardness and wear resistance in Ni–W alloy coatings, Surf. Coating. Technol. 206 (2011) 1096.
[20] M. Metikos-Hukovic, Z. Grubac, N. Radic, A. Tonejc, Sputter deposited nanocrystalline Ni and Ni-W films as catalysts for hydrogen evolution, J. Mol. Catal. A Chem. 249 (2006) 172.
[21] M. Lagarde, A. Billard, J. Creus, X. Feaugas, J.L. Grosseau-Poussard, S. Touzain, C. Savall, Electrochemical behavior of Ni W alloys obtained by magnetron sputtering, Surf. Coating. Technol. 352 (2018) 581.
[22] J.M.V. Nsanzimana, Y. Peng, M. Miao, V. Reddu, W. Zhang, H. Wang, B.Y. Xia, X. Wang, An earth-abundant tungsten–nickel alloy electrocatalyst for superior hydrogen evolution, ACS Appl. Nano Mater. 1 (2018) 1228.
[23] F. Rosalbino, D. Maccio, A. Saccone, G. Scavino, Study of Co–W crystalline alloys as hydrogen electrodes in alkaline water electrolysis, Int. J. Hydrogen Energy 39 (2014) 12448.
[24] T. Nasu, M. Sakurai, T. Kamiyama, T. Usuki, O. Uemura, K. Tokumitsu, T. Yamasaki, Structural comparison of M–W (M = Fe, Ni) alloys produced by electrodeposition and mechanical alloying, Mater. Sci. Eng. A 375–377 163. (2004)
[25] T.D. Shen, K.Y. Wang, M.X. Quan, J.T. Wang, Amorphous phase transition mechanism by the mechanical alloying of the Fe–W system, J. Appl. Phys. 71 (1992) 1967.
[26] A. Genç, M.L. Oveçoglu, M. Baydogan, S. Turan, Fabrication and characterization of Ni–W solid solution alloys via mechanical alloying and pressureless sintering, Mater. Des. 42 (2012) 495.
[27] M.A. Domínguez-Crespo, M. Plata-Torres, A.M. Torres-Huerta, E.M. Arce-Estrada, J.M. Hallen-L´opez, Kinetic study of hydrogen evolution reaction on $Ni_{30}Mo_{70}$, C o $_{30}Mo_{70}$, C o $_{30}Ni_{70}$ and $Co_{10}Ni_{20}Mo_{70}$ alloy electrodes, Mater. Char. 55 (2005) 83.
[28] H. Alimadadi, M. Ahmadi, M. Aliofkhazraei, S.R. Younesi, Corrosion properties of electrodeposited nanocrystalline and amorphous patterned Ni–W alloy, Mater. Des. 30 (2009) 1356.
[29] A. Nicolenco, N. Tsyntsaru, H. Cesiulis, Fe (III)-based ammonia-free bath for electrodeposition of Fe-W alloys, J. Electrochem. Soc. 164 (2017) D590.
[30] D.P. Weston, S.J. Harris, P.H. Shipway, N.J. Weston, G.N. Yap, Establishing relationships between bath chemistry, electrodeposition and microstructure of Co–W alloy coatings produced from a gluconate bath, Electrochim. Acta 55 (2010) 5695.
[31] G. Abuin, R. Coppola, L. Diaz, Ni-Mo alloy electrodeposited over Ni substrate for HER on water electrolysis, Electrocatalysis 10 (2019) 17.
[32] C. Fan, D.L. Piron, A. Sleb, P. Paradis, Study of electrodeposited nickel-molybdenum, nickel-tungsten, cobalt-molybdenum, and cobalt-tungsten as hydrogen electrodes in alkaline water electrolysis, J. Electrochem. Soc. 141 (1994) 382.
[33] N. Tsyntsaru, A. Dikusar, H. Cesiulis, J.P. Celis, Z. Bobanova, S. Sidelnikova, S. Belevskii, Y. Yapontseva, O. Bersirova, V. Kublanovskii, Tribological and corrosive characteristics of electrochemical coatings based on cobalt and iron superalloys, Powder Metall. Met. Ceram. 48 (2009) 419.
[34] M. Benaicha, M. Allam, A. Dakhouche, M. Hamla, Electrodeposition and characterization of W-rich NiW alloys from citrate electrolyte, Int. J. Electrochem. Sci. 11 (2016) 7605.
[35] S.H. Hong, S.H. Ahn, J. Choi, J.Y. Kim, H.Y. Kim, H.-J. Kim, J.H. Jang, H. Kim, S.-K. Kim, High-activity electrodeposited NiW catalysts for hydrogen evolution in alkaline water electrolysis, Appl. Surf. Sci. 349 (2015) 629.
[36] V.S. Kublanovsky, Y.S. Yapontseva, Electrocatalytic properties of Co-Mo alloys electrodeposited from a citrate-pyrophosphate electrolyte, Electrocatalysis 5 (2014) 372.
[37] M. Wang, Z. Wang, Z. Guo, Z. Li, The enhanced electrocatalytic activity and stability of NiW films electrodeposited under super gravity field for hydrogen evolution reaction, Int. J. Hydrogen Energy 36 (2011) 3305.
[38] H. Cesiulis, N. Tsyntsaru, A. Budreika, N. Skridaila, Electrodeposition of CoMo and CoMoP alloys from the weakly acidic solutions, Электронная обработка материалов 5 (2010) 17.
[39] S. Voskanyan, G. Pchelarov, R. Rashkov, K. Petrov, Co and W alloys as catalysts for evolution of H_2 at elevated temperatures, Bulg. Chem. Commun. 48 (2016) 78.
[40] N. Tsyntsaru, H. Cesiulis, E. Pellicer, J.P. Celis, J. Sort, Structural, magnetic, and mechanical properties of electrodeposited cobalt–tungsten alloys: intrinsic and extrinsic interdependencies, Electrochim. Acta 104 (2013) 94.
[41] M. Donten, H. Cesiulis, Z. Stojek, Electrodeposition and properties of Ni-W, Fe-W and Fe-Ni-W amorphous alloys. A comparative study, Electrochim. Acta 45 (2000) 3389.
[42] B.D. Cullity, S.R. Stock, Elements of X-Ray Diffraction, third ed., Prentice Hall, Upper Saddle River, New Jersey, 2001.
[43] H. Kahlert, Reference electrodes, in: F. Scholz (Ed.), Electroanalytical Methods, Springer, Berlin, Heidelberg, 2005, p. 261.
[44] S.H. Ahn, I. Choi, H.Y. Park, S.J. Hwang, S.J. Yoo, E. Cho, H.J. Kim, D. Henkensmeier, S.W. Nam, S.K. Kim, J.H. Jang, Effect of morphology of electrodeposited Ni catalysts on the behavior of bubbles generated during the oxygen evolution reaction in alkaline water electrolysis, Chem. Commun. 49 (2013) 9323.
[45] L. Elias, P. Cao, A.C. Hegde, Magnetoelectrodeposition of Ni-W alloy coatings for enhanced hydrogen evolution reaction, RSC Adv. 6 (2016) 111358.
[46] K. Mech, P. Zabinski, M. Mucha, R. Kowalik, Electrodeposition of catalytically active Ni-Mo Alloys, Arch. Metall. Mater. 58 (2013) 227.
[47] J. Jaksic, M. Vojnovic, N. Krstajic, Kinetic analysis of hydrogen evolution at Ni–Mo alloy electrodes, Electrochim. Acta 45 (2000) 4151.
[48] N. Tsyntsaru, H. Cesiulis, M. Donten, J. Sort, E. Pellicer, E.J. Podlaha-Murphy, Modern trends in tungsten alloys electrodeposition with iron group metals, Surf. Eng. Appl. Electrochem. 48 (2012) 491.
[49] T. Yamasaki, P. Schloßmacher, K. Ehrlich, Y. Ogino, Formation of amorphous electrodeposited Ni-W alloys and their nanocrystallization, Nanostruct. Mater. 10 (1998) 375.
[50] M. Donten, Z. Stojek, H. Cesiulis, Formation of nanofibers in thin layers of amorphous W alloys with Ni, Co, and Fe obtained by electrodeposition, J. Electrochem. Soc. 150 (2003) C95.
[51] K.H. Hou, Y.F. Chang, S.M. Chang, C.H. Chang, The heat treatment effect on the structure and mechanical properties of electrodeposited nano grain size Ni–W alloy coatings, Thin Solid Films 518 (2010) 7535.
[52] S. Lee, M. Choi, S. Park, H. Jung, B. Yoo, Mechanical properties of electrodeposited Ni-W thin films with alternate W-rich and W-poor multilayers, Electrochim. Acta 153 (2015) 225.
[53] Th Borucinski, S. Rausch, H. Wendt, Raney nickel activated H_2-electrodes Part II: correlation of morphology and effective catalytic activity of Raney-nickel coated cathodes, J. Appl. Electrochem. 22 (1992) 1031.
[54] L. Elias, A.C. Hegde, Electrodeposition and electrocatalytic etudy of Ni-W alloy coating, Mater. Sci. Forum 830–831 (2015) 651.
[55] Y. Wu, Q. Luo, J. Jiao, X. Wei, J. Shen, Investigating the wear behavior of Fe-based amorphous coatings under nanoscratch tests, Metals 7 (2017) 118.
[56] S. Yao, S. Zhao, H. Guo, M. Kowaka, A new amorphous alloy deposit with high corrosion resistance, Corrosion 52 (1996) 183.
[57] A. Nicolenco, N. Tsyntsaru, J. Fornell, E. Pellicer, J. Reklaitis, D. Baltrunas, H. Cesiulis, J. Sort, Mapping of magnetic and mechanical properties of Fe-W alloys electrodeposited from Fe(III)-based glycolate-citrate bath, Mater. Des. 139 (2018) 429.
[58] F. Su, C. Liu, Q. Zuo, P. Huang, M. Miao, A comparative study of electrodeposition techniques on the microstructure and property of nanocrystalline cobalt deposit, Mater. Chem. Phys. 139 (2013) 663.
[59] F. Su, C. Liu, P. Huang, Friction and wear of nanocrystalline Co and Co–W alloy coatings produced by pulse reverse electrodeposition, Wear 300 (2013) 114.
[60] H. Okamoto, Ni-W(Nickel-Tungsten), J. Phase Equilibria 12 (1991) 706.
[61] H. Okamoto, Co-W (Cobalt-Tungsten), J. Phase Equilibria Diffusion 29 (2008) 119.
[62] B. Predel, Fe-W (Iron-Tungsten), in: O. Madelung (Eds.), Dy-Er – Fr-Mo, Vol.

vol. 5, Springer, Berlin, Heidelberg, p. 1.

[63] M. Donten, Bulk and surface composition, amorphous structure, and thermocrystallization of electrodeposited alloys of tungsten with iron, nickel, and cobalt, J. Solid State Electrochem. 3 (1999) 87.

[64] T.M. Sridhar, N. Eliaz, E. Gileadi, Electroplating of Ni_4W, Electrochem. Solid State Lett. 8 (2005) C58.

[65] M.M. Jaksic, Advances in electrocatalysis for hydrogen evolution in the light of the Brewer-Engel valence-bond theory, J. Mol. Catal. 38 (1986) 161.

[66] M.M. Jaksic, Electrocatalysis of hydrogen evolution in the light of the brewer—engel theory for bonding in metals and intermetallic phases, Electrochim. Acta 29 (1984) 1539.

[67] L. Elias, K. Scott, A.C. Hegde, Electrolytic synthesis and characterization of electrocatalytic Ni-W alloy, J. Mater. Eng. Perform. 24 (2015) 4182.

[68] V.V. Kuznetsov, A.A. Kalinkina, T.V. Pshenichkina, V.V. Balabaev, Electrocatalytic properties of cobalt-molybdenum alloy deposits in the hydrogen evolution reaction, Russ. J. Electrochem. 44 (2008) 1350.

[69] G.S. Tasic, U. Lacnjevac, M.M. Tasic, M.M. Kaninski, V.M. Nikolic, D.L. Zugic, V.D. Jovic, Influence of electrodeposition parameters of Ni−W on Ni cathode for alkaline water electrolyser, Int. J. Hydrogen Energy 38 (2013) 4291.

[70] T. Shinagawa, A.T. Garcia-Esparza, K. Takanabe, Insight on Tafel slopes from a microkinetic analysis of aqueous electrocatalysis for energy conversion, Sci. Rep. 5 (2015) 13801.

[71] Q. Ding, B. Song, P. Xu, S. Jin, Efficient electrocatalytic and photoelectrochemical hydrogen generation using MoS_2 and Related Compounds, Chem 1 (2016) 699.

[72] M. Stancheva, S. Manev, D. Lazarov, M. Mitov, Catalytic activity of nickel based amorphous alloys for oxidation of hydrogen and carbon monoxide, Appl. Catal. Gen. 135 (1996) L19.

[73] M. Armbrüster, R. Schlogl, Y. Grin, Intermetallic compounds in heterogeneous catalysis—a quickly developing field, Sci. Technol. Adv. Mater. 15 (2014) 034803

[74] S. Martinez, M. Metikos-Hukovic, L. Valek, Electrocatalytic properties of electrodeposited Ni−15Mo cathodes for the HER in acid solutions: synergistic electronic effect, J. Mol. Catal. A Chem. 245 (2006) 114.

[75] C. Gonzalez-Buch, I. Herraiz-Cardona, E.M. Ortega, J. García-Anton, V. Perez-Herranz, Development of Ni-Mo, Ni-W and Ni-Co macroporous materials for hydrogen evolution reaction, Chem. Eng. Trans. 32 (2013) 865.

[76] G. Lu, P. Evans, G. Zangari, Electrocatalytic properties of Ni-based alloys toward hydrogen evolution reaction in acid media, J. Electrochem. Soc. 150 (2003) A551.

[77] J. Zhang, T. Wang, P. Liu, Z. Liao, S. Liu, X. Zhuang, M. Chen, E. Zschech, X. Feng, Efficient hydrogen production on $MoNi_4$ electrocatalysts with fast water dissociation kinetics, Nat. Commun. 8 (2017) 15437.

[78] J. Hou, Y. Wu, S. Cao, Y. Sun, L. Sun, Active sites intercalated ultrathin carbon sheath on nanowire arrays as integrated core-shell architecture: highly effi-cient and durable electrocatalysts for overall water splitting, Small 13 (2017) 1702018.

[79] E. Soghrati, C. Kok Poh, Y. Du, F. Gao, S. Kawi, A. Borgna, C−O hydrogenolysis of tetrahydrofurfuryl alcohol to 1,5-pentanediol over bi-functional nickel-tungsten catalysts, ChemCatChem 10 (2018) 4652.

[80] S.E. Fosdick, S.P. Berglund, C.B. Mullins, R.M. Crooks, Evaluating electrocatalysts for the hydrogen evolution reaction using bipolar electrode arrays: bi- and trimetallic combinations of Co, Fe, Ni, Mo, and W, ACS Catal. 4 (2014) 1332.

[81] D. Goranova, E. Lefterova, R. Rashkov, Electrocatalytic activity of Ni-Mo-Cu and Ni-Co-Cu alloys for hydrogen evolution reaction in alkaline medium, Int. J. Hydrogen Energy 42 (2017) 28777.

[82] A.W. Jeremiasse, J. Bergsma, J.M. Kleijn, M. Saakes, C.J.N. Buisman, M. Cohen Stuart, H.V.M. Hamelers, Performance of metal alloys as hydrogen evolution reaction catalysts in a microbial electrolysis cell, Int. J. Hydrogen Energy 36 (2011) 10482.

[83] S.S. Brenner, Oxidation of iron-molybdenum and nickel-molybdenum alloys, J. Electrochem. Soc. 102 (1955) 7.

[84] H. Yildirim, H. Morcali, A. Turan, Nickel pig iron (NPI) production from lateritic nickel ores, in: 13th International Ferro Alloys Congress, Almaty, Kazakhstan, 2013, p. 8, 9-13 June.

[85] E. Navarro-Flores, Z. Chong, S. Omanovic, Characterization of Ni, NiMo, NiW and NiFe electroactive coatings as electrocatalysts for hydrogen evolution in an acidic medium, J. Mol. Catal. A Chem. 226 (2005) 179.

[86] T. Boiadjieva-Scherzer, H. Kronberger, G. Fafilek, M. Monev, Hydrogen evolution reaction on electrodeposited Zn-Cr alloy coatings, J. Electroanal. Chem. 783 (2016) 68.

[87] P.N.S. Casciano, R.L. Benevides, R.A.C. Santana, A.N. Correia, P. de Lima-Neto, Factorial design in the electrodeposition of Co-Mo coatings and their evaluations for hydrogen evolution reaction, J. Alloy. Comp. 723 (2017) 164.

[88] M.P.Q. Arganaraz, S.B. Ribotta, M.E. Folquer, L.M. Gassa, G. Benítez, M.E. Vela, R.C. Salvarezza, Ni−W coatings electrodeposited on carbon steel: chemical composition, mechanical properties and corrosion resistance, Electrochim. Acta 56 (2011) 5898.

[89] M. Sheng, W. Weng, Y. Wang, Q. Wu, S. Hou, Co-W/CeO_2 composite coatings for highly active electrocatalysis of hydrogen evolution reaction, J. Alloy. Comp. 743 (2018) 682.

[90] T. Zheng, W. Sang, Z. He, Q. Wei, B. Chen, H. Li, C. Cao, R. Huang, X. Yan, B. Pan, S. Zhou, J. Zeng, Conductive tungsten oxide nanosheets for highly efficient hydrogen evolution, Nano Lett. 17 (12) (2017) 7968, 13.